Cell Reports

Article

# TIM23 facilitates PINK1 activation by safeguarding against OMA1-mediated degradation in damaged mitochondria

## Graphical abstract

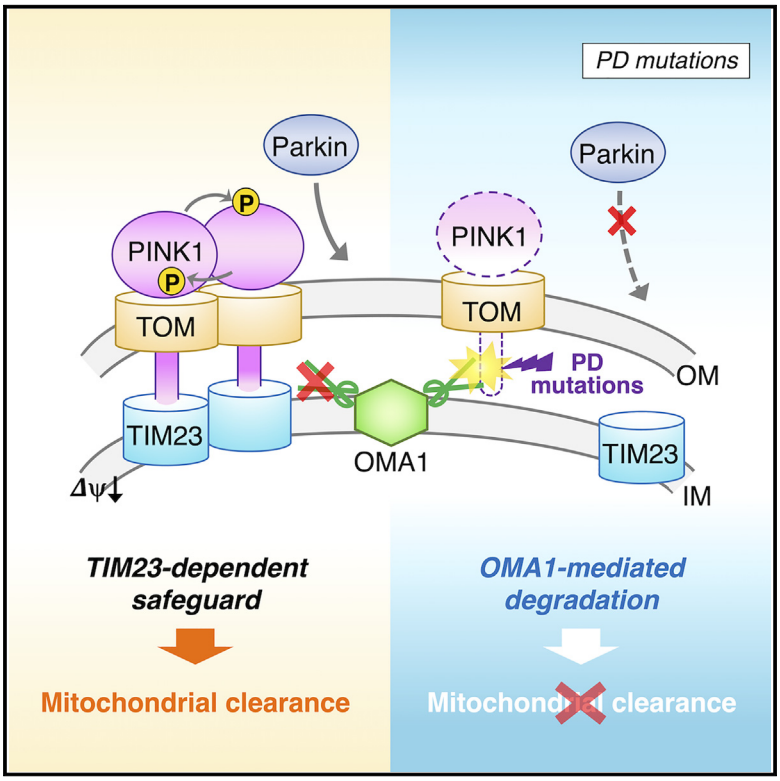


## Authors

Shiori Akabane, Kiyona Watanabe, Hidetaka Kosako, ..., Noriyuki Matsuda, Toshiya Endo, Toshihiko Oka

## Correspondence

toka@rikkyo.ac.jp

## In brief

Akabane et al. show that TIM23 is a component of the PINK1-containing protein complex and safeguards PINK1 against OMA1-dependent degradation in damaged mitochondria, indicating that TIM23 plays a distinct role in facilitating PINK1 activation and subsequent mitochondrial clearance.

## Highlights

- The mitochondrial translocase TIM23 is identified as a member of the PINK1 complex
- Inactivation of TIM23 leads to a reduction in PINK1 and mislocalization of Parkin
- TIM23 prevents OMA1 from degrading PINK1 in damaged mitochondria
- Some pathogenic PINK1 mutations impair interactions with PINK1 and TIM23

Akabane et al., 2023, Cell Reports *42*, 112454
May 30, 2023 
https://doi.org/10.1016/j.celrep.2023.112454

CellPress

Cell Reports

CellPress
OPEN ACCESS

Article

# TIM23 facilitates PINK1 activation by safeguarding against OMA1-mediated degradation in damaged mitochondria

Shiori Akabane,[1,2] Kiyona Watanabe,[1] Hidetaka Kosako,[3] Shun-ichi Yamashita,[4] Kohei Nishino,[3] Masahiro Kato,[1] Shiori Sekine,[5] Tomotake Kanki,[4] Noriyuki Matsuda,[6] Toshiya Endo,[2,7] and Toshihiko Oka[1,8,*]

[1]Department of Life Science, Rikkyo University, Tokyo 171-8501, Japan
[2]Faculty of Life Sciences, Kyoto Sangyo University, Kyoto 603-8555, Japan
[3]Division of Cell Signaling, Fujii Memorial Institute of Medical Sciences, Tokushima University, Tokushima 770-8503, Japan
[4]Department of Cellular Physiology, Niigata University Graduate School of Medical and Dental Sciences, Niigata 951-8510, Japan
[5]Aging Institute, Division of Cardiology, Department of Medicine, University of Pittsburgh, Pittsburgh, PA 15219, USA
[6]Biomolecular Pathogenesis, Medical Research Institute, Tokyo Medical and Dental University, Tokyo 113-8519, Japan
[7]Institute for Protein Dynamics, Kyoto Sangyo University, Kyoto 603-8555, Japan
[8]Lead contact
*Correspondence: toka@rikkyo.ac.jp
https://doi.org/10.1016/j.celrep.2023.112454

## SUMMARY

PINK1 is activated by autophosphorylation and forms a high-molecular-weight complex, thereby initiating the selective removal of damaged mitochondria by autophagy. Other than translocase of the outer mitochondrial membrane complexes, members of PINK1-containing protein complexes remain obscure. By mass spectrometric analysis of PINK1 co-immunoprecipitates, we identify the inner membrane protein TIM23 as a component of the PINK1 complex. TIM23 downregulation decreases PINK1 levels and significantly delays autophosphorylation, indicating that TIM23 promotes PINK1 accumulation in response to depolarization. Moreover, inactivation of the mitochondrial protease OMA1 not only enhances PINK1 accumulation but also represses the reduction in PINK1 levels induced by TIM23 downregulation, suggesting that TIM23 facilitates PINK1 activation by safeguarding against degradation by OMA1. Indeed, deficiencies of pathogenic PINK1 mutants that fail to interact with TIM23 are partially restored by OMA1 inactivation. These findings indicate that TIM23 plays a distinct role in activating mitochondrial autophagy by protecting PINK1.

## INTRODUCTION

Genetic studies of familial Parkinson's disease (PD) led to the identification of more than 16 causal genes that are dominantly or recessively inherited.[1,2] Among the genetic alterations, several mutations in the *PARK6* gene encoding PTEN-induced kinase 1 (PINK1) are highly associated with hereditary cases, and pathogenic PINK1 variants have been well characterized by genetic, biochemical, and molecular biological approaches,[3–5] revealing that PINK1 has a central role as a sensor in surveying mitochondrial quality. PINK1 is newly synthesized in the cytosol, delivered to energized mitochondria, translocated across the mitochondrial outer membrane (MOM) through translocase of the outer mitochondrial membrane (TOM) machinery, and inserted into the mitochondrial inner membrane (MIM) via a translocase of the inner mitochondrial membrane complex containing TIM23. The inner membrane protease PARL catalyzes proteolytic cleavage of the PINK1 transmembrane domain, resulting in retrotranslocational release of the truncated PINK1 from the mitochondria followed by its proteasomal degradation in the cytoplasm.[6,7]

In damaged mitochondria, dissipation of the mitochondrial membrane potential ($\Delta\psi m$) impairs the insertion of PINK1 into the MIM, compromising the subsequent proteolytic cleavage. Consequently, PINK1 accumulates on the MOM and then, together with the TOM complex, forms a protein complex with a high molecular weight of more than 850 kDa, which leads to the autophosphorylation required for its ubiquitin kinase activity.[8–10] PINK1-mediated phosphorylation of ubiquitin conjugated on MOM proteins triggers the mitochondrial recruitment of Parkin, a product of another causal gene (*PARK2*) associated with familial forms of PD. Subsequently, the ubiquitin-like domain of Parkin localized on the MOM is also phosphorylated by PINK1, uncovering the hidden ubiquitin ligase activity of Parkin.[11–13] PINK1- and Parkin-dependent modification of the phospho-ubiquitin chains on MOM proteins enhances the mitochondrial recruitment of Parkin, eventually inducing the NDP52- and optineurin-mediated autophagy that selectively eliminates damaged mitochondria.[14,15]

The TIM23 complex has an intrinsic function to promote both the translocation of preproteins across the MIM and their insertion into the MIM.[16–18] TIM23 is a core subunit forming the

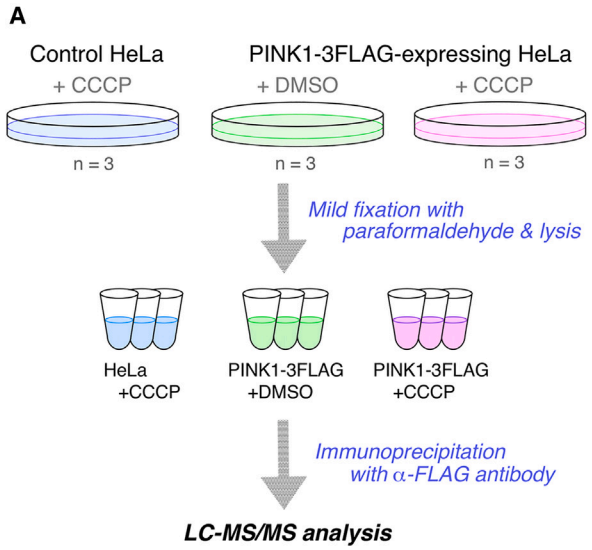


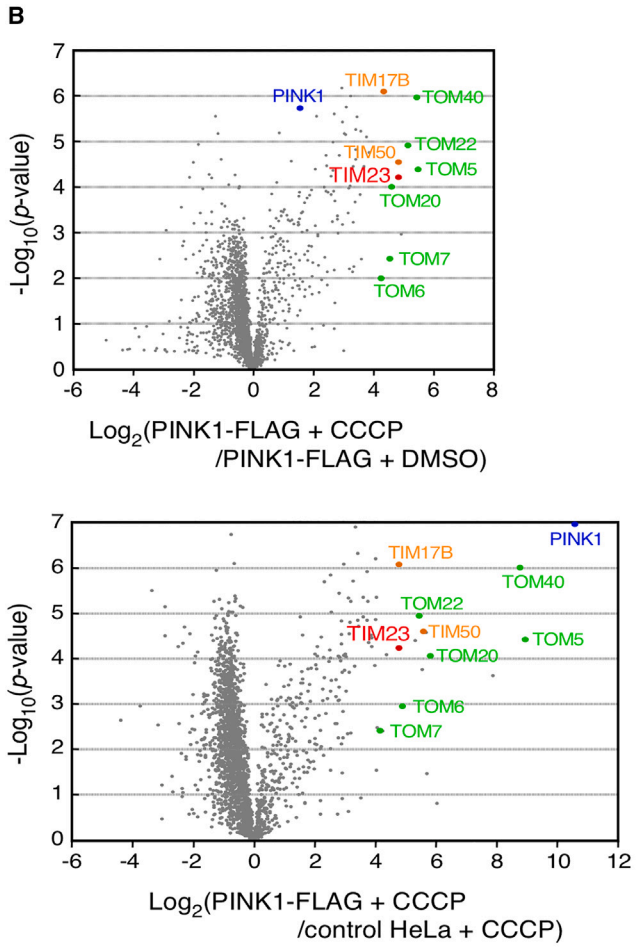


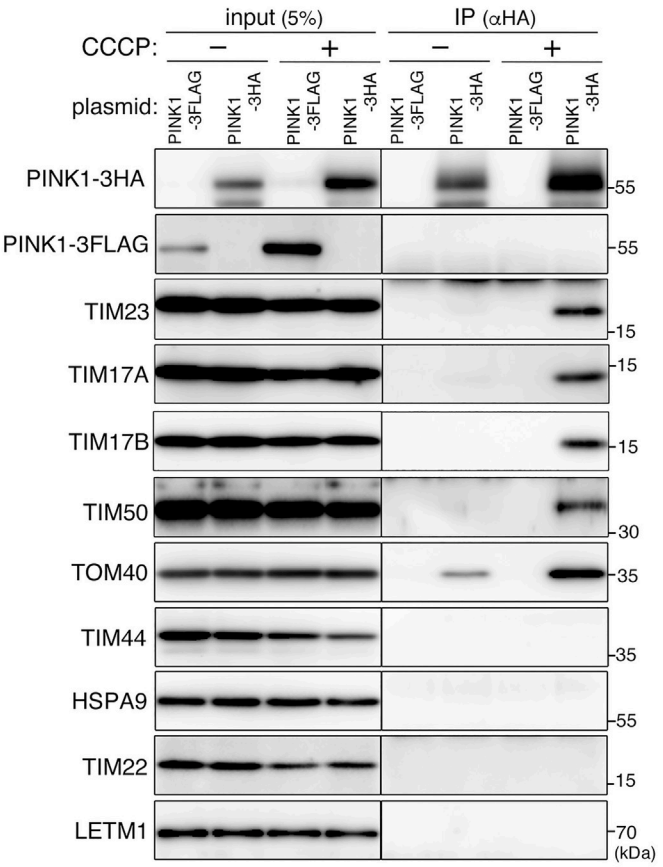


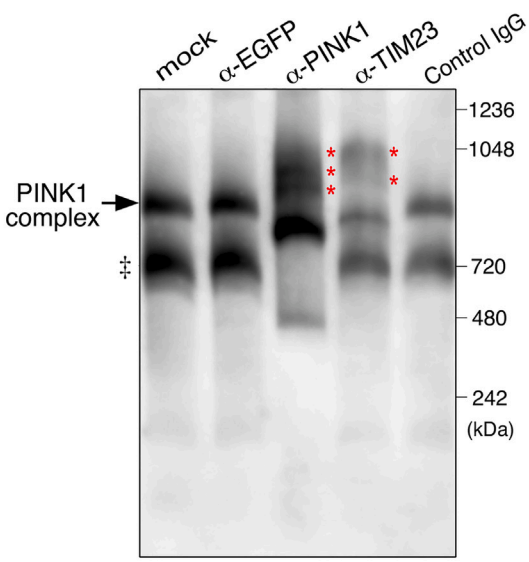


(legend on next page)

channel pore and associates with respiratory chains in a TIM21-dependent manner.[19] The insertion of precursors into the MIM requires a change in the $\Delta\psi m$ across the MIM, and protein translocation into the matrix further requires an additional driving force generated by the ATP-dependent presequence translocase-associated import motor.[18] The $\Delta\psi m$, in addition to matrix-targeting sequences, is necessary for activating the channel formed by the TIM23 complex.[16,17] Because TIM23-mediated translocation and insertion depend exclusively on the $\Delta\psi m$, the roles of TIM23 in mitochondria without the $\Delta\psi m$ remain obscure. Here, we demonstrated that TIM23 is incorporated into the PINK1-containing protein complex, and some pathogenic PINK1 mutations interrupt its association with TIM23. TIM23 knockdown (KD) decreased PINK1 levels and impaired PINK1 autophosphorylation. Furthermore, downregulation of OMA1, a stress-activated protease, enhanced the accumulation of PINK1 on the MOM and suppressed the decrease in PINK1 levels induced by TIM23 inactivation. Overall, these findings indicate that TIM23 prevents OMA1 from rapidly degrading PINK1 in mitochondria without $\Delta\psi m$, thereby promoting the selective elimination of damaged mitochondria.

## RESULTS

### TIM23 is incorporated into the PINK1 complex in response to mitochondrial depolarization

To identify proteins incorporated into the PINK1-containing protein complex in response to mitochondrial depolarization, cells stably expressing PINK1-3FLAG were treated with or without the protonophore carbonyl cyanide *m*-chlorophenyl hydrazone (CCCP), moderately crosslinked with paraformaldehyde, and immunoprecipitated with anti-FLAG antibody. The co-precipitated proteins were analyzed by liquid chromatography-tandem mass spectrometry (LC-MS/MS) (Figure 1A). Consistent with previous reports,[8,9] subunits of the TOM complex clearly co-precipitated with PINK1-3FLAG upon CCCP treatment. Of the ten most abundant proteins in the CCCP-treated samples, six were TOM complex subunits (TOM40, TOM22, TOM20, TOM7, TOM6, and TOM5) (Figure 1B and Table S1). Interestingly, three of the remaining proteins were TIM23 complex subunits (TIM23, TIM50, and TIM17B). TIM23 is a core subunit of the complex and forms the channel pore for protein translocation across the MIM;[16,18] therefore, TIM23 was further investigated.

To confirm the interaction of PINK1 with TIM23 in depolarized mitochondria, cells were transfected with expression plasmids for either PINK1-3HA or PINK1-3FLAG, incubated with or without CCCP, and solubilized by digitonin without paraformaldehyde pretreatment. The resulting solubilized samples were immunoprecipitated with anti-HA antibody. In response to depolarization, PINK1-3HA, but not PINK1-3FLAG, clearly co-precipitated with TIM23 (Figure 1C). Other subunits of the TIM23 core complex (TIM50, TIM17A, and TIM17B) were also detectable in the CCCP-treated cells, whereas components of the TIM23-associated import motor (TIM44 and HSPA9) were barely observed. TIM22, a core subunit of another translocase complex across the MIM, and LETM1, a MIM protein, were undetectable in the immunoprecipitated samples. ATP depletion did not influence the interaction of PINK1 with TIM23 (Figure S1A), consistent with the absence of ATP-dependent import motor subunits (TIM44 and HSPA9). The results indicated that PINK1 bound specifically to TIM23 and the other core subunits in depolarized mitochondria. Moreover, to quantify protein levels of TIM23 co-precipitated by PINK1-3HA in CCCP-treated cell lysates, the immunoprecipitated proteins were digested by trypsin and subjected to absolute quantification peptide-based quantitative MS analysis (Figure S1B and Table S2). Three different peptides derived from the precipitated TIM23 were detected in the range of 3.3–13.7 fmol, and three peptides derived from PINK1-3HA were recovered in the range of 21.5–63.4 fmol. Considering the dissociation of TIM23 during the immunoprecipitation procedures and the efficiency of trypsin digestion, the result suggests that interactions between PINK1 and TIM23 in cells occur at a comparable range of protein levels.

To examine whether MOM-localized PINK1 associated with TIM23, we used a PINK1 fusion protein containing the tobacco etch virus (TEV) protease-specific site (TEV site) between the hemagglutinin (HA) tag and green fluorescent protein (PINK1-3HA-TEV site-GFP) and a mitochondrial intermembrane space protein MIC19-3HA fused to the TEV site and FLAG tag (MIC19-3HA-TEV site-3FLAG; Figure S1C). The mitochondrial fraction prepared from cells expressing both PINK1-3HA-TEV site-GFP and MIC19-3HA-TEV site-3FLAG was subjected to cleavage with TEV protease. PINK1-3HA-TEV site-GFP was completely processed to PINK1-3HA, whereas most of the MIC19-3HA-TEV site-3FLAG was resistant to TEV protease (Figure S1D), indicating that PINK1-3HA-TEV site-GFP is localized on the MOM and usually exposed to the cytosol. Using the mitochondrial fraction treated with or without TEV protease, the PINK1 fusion protein was immunoprecipitated. TEV-cleaved PINK1-3HA efficiently co-precipitated with TIM23 (Figure S1E). These results strongly showed that PINK1 localized on the

**Figure 1. Identification of TIM23 as a component of the PINK1 protein complex**

(A) Scheme for LC-MS/MS analysis of co-immunoprecipitates with PINK1-3FLAG. Control and PINK1-3FLAG-expressing cells treated with CCCP or DMSO were moderately fixed with 0.1% paraformaldehyde, solubilized, immunoprecipitated with an anti-FLAG antibody, and subjected to LC-MS/MS analysis.

(B) Volcano plots represent abundance ratios plotted against the p value for three independent experiments (upper panel, CCCP vs. DMSO; lower panel, PINK1-3FLAG-expressing cells vs. control cells). Red, orange, green, and blue dots indicate TIM23, other TIM23 complex subunits, TOM complex subunits, and PINK1, respectively.

(C) Cells transfected with expression plasmid carrying PINK1-3HA or PINK1-3FLAG were treated with CCCP, solubilized with digitonin, and immunoprecipitated (IP) with an anti-HA antibody, followed by immunoblot analysis. Input, 5% of solubilized cell lysates.

(D) Digitonin-solubilized mitochondrial fractions were prepared from CCCP-treated cells stably expressing PINK1-3FLAG, incubated with the indicated antibodies, and analyzed by CN-PAGE and immunoblotting with an anti-FLAG antibody. Asterisks indicate shifted bands. Arrow denotes the PINK1-3FLAG-containing protein complex. Double dagger represents an additional complex that depends on the expression levels of PINK1-3FLAG.

See also Figure S1.

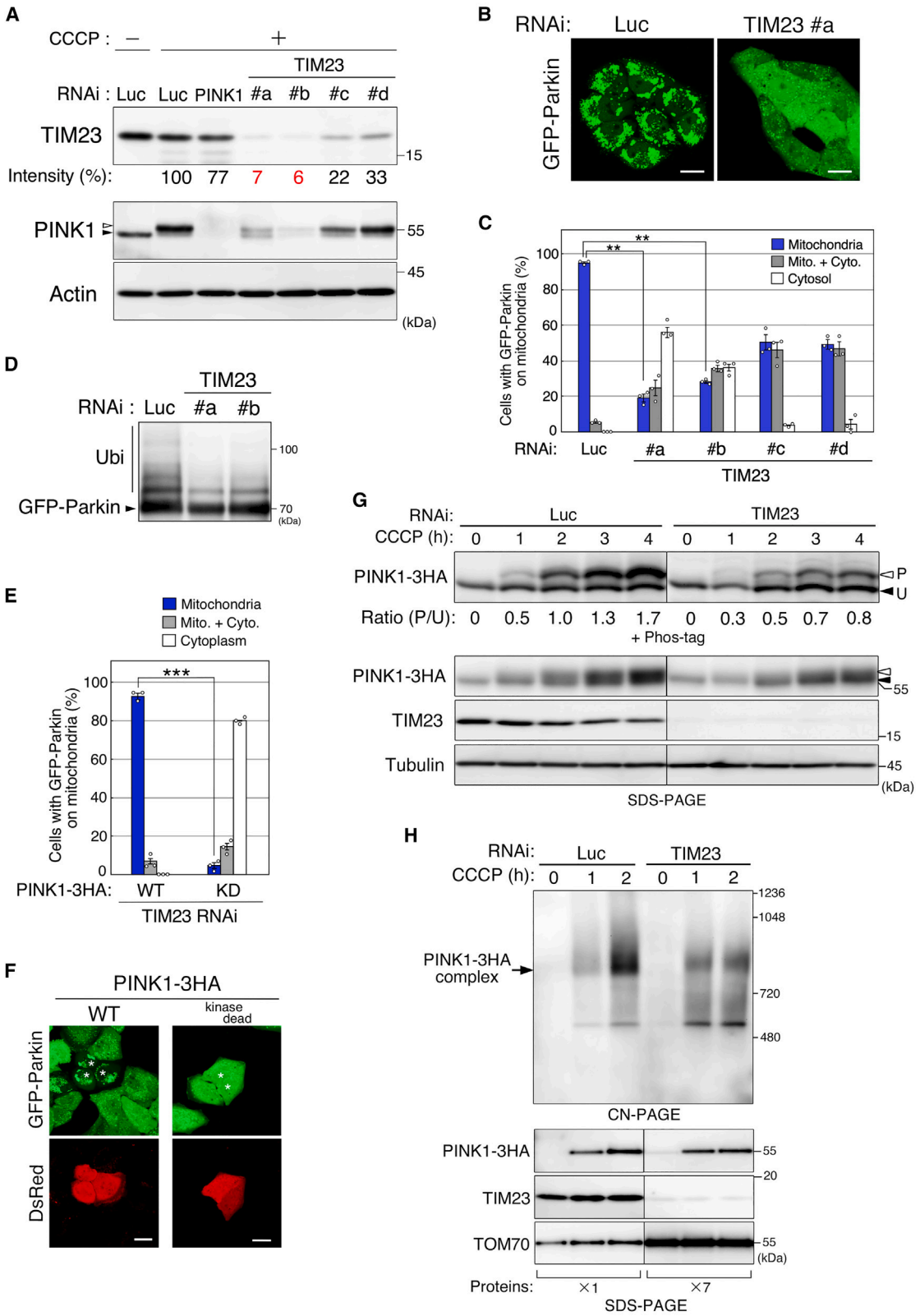


*(legend on next page)*

MOM, but not PINK1 present inside the mitochondria, interacts with TIM23.

We further performed a native antibody-based mobility shift (NAMOS) assay to evaluate whether the PINK1 complex contained TIM23. Mitochondrial fractions prepared from PINK1-3FLAG-expressing cells were solubilized with digitonin and incubated with antibodies to either TIM23, PINK1, or enhanced GFP, followed by clear-native polyacrylamide gel electrophoresis (CN-PAGE) and immunoblot analysis. Multiple mobility shifts in the PINK1 complexes were detected by adding anti-TIM23 antibody as well as anti-PINK1 antibody (Figure 1D, asterisks), indicating that TIM23 is a component of the PINK1 complex.

## TIM23 is required for PINK1 accumulation on depolarized mitochondria

TIM23 plays a critical role in protein translocation into mitochondria and is therefore indispensable for cell growth and embryogenesis.[20,21] To investigate the role of TIM23 in mitochondrial quality control, we carefully knocked down TIM23 expression using four different small interference RNAs (siRNAs) (#a–#d). Each siRNA decreased TIM23 protein at a steady-state level (Figures 2A and S2A). In particular, two of the siRNAs (#a and #b) induced a more than 91% reduction in TIM23 expression. Transfection with each siRNA induced mitochondrial fragmentation and delayed cell growth to varying degrees (Figures S2D and S2F). Next, we assessed the effect of the siRNAs on the TIM23 function by monitoring mitochondrial import of a matrix-targeted GFP (mito-GFP) into energized mitochondria. Strong inhibition of mitochondrial import was observed when transfected with either of two siRNAs (#a and #b). The other siRNAs (#c and #d) did not significantly inhibit the mito-GFP translocation (Figures S2B and S2C). In addition to mito-GFP, introduction of the siRNAs (#a and #b) induced a significant accumulation of precursors of matrix proteins (HSPD1 and ATP5A1) and slightly enhanced the proteolytic processing of OPA1 (Figure S2H). The results indicated that a more than 90% reduction in TIM23 levels was required to efficiently interfere with TIM23-mediated protein import across the MIM. Thus, even a small portion (~10%) of TIM23 protein in cells may be sufficient to drive protein translocation.

Next, we evaluated the effect of TIM23 KD on PINK1 protein levels in depolarized mitochondria. Cells transfected with control siRNA (luciferase) or TIM23 siRNAs were treated with CCCP and subjected to immunoblot analysis. Transfection with two of the TIM23 siRNAs (#a and #b) drastically reduced PINK1 protein levels, while transfection with the other two siRNAs induced no significant change in the PINK1 amount (Figure 2A), consistent with the results of mitochondrial import of mito-GFP, HSPD1, and ATP5A1 (Figures S2B, S2C, and S2H). Quantitative PCR analysis of PINK1 transcripts revealed that none of the TIM23 siRNAs significantly influenced PINK1 mRNA levels (Figure S2E). Parkin is selectively recruited to depolarized mitochondria in a PINK1-dependent manner.[22,23] Although transfection with each TIM23 siRNA moderately decreased the $\Delta\psi m$, the decrease was not sufficient to induce obvious mitochondrial localization of GFP-Parkin without CCCP treatment (Figure S2G). Upon CCCP treatment, recruitment of GFP-Parkin to depolarized mitochondria was clearly observed in control siRNA-transfected cells. In contrast, transfection with either of two siRNAs (#a and #b) strongly inhibited GFP-Parkin recruitment (Figures 2B and 2C). We further analyzed the conjugation of polyubiquitin chains onto GFP-Parkin because Parkin recruitment to the MOM eventually unveils its latent enzymatic activity,[23] i.e., autoubiquitination of GFP-Parkin is an indicator of mitochondrial localization. Autoubiquitination of GFP-Parkin clearly decreased following transfection with the same siRNAs (Figure 2D). These results indicated that strong interference with TIM23 function by these siRNAs led to a failure of PINK1 accumulation on depolarized mitochondria and the mislocalization of Parkin. Moreover, ectopic expression of siRNA-insensitive TIM23-3HA suppressed the deficiency in mitochondrial recruitment of GFP-Parkin in TIM23-KD cells (Figure S2I), indicating that Parkin mislocalization is caused by gene silencing of TIM23. A previous study reported that TIM23 KD did not significantly influence Parkin recruitment in a cell line stably expressing yellow fluorescence protein (YFP)-Parkin.[24] Immunoblot analysis showed that YFP-Parkin in the cell line used in the previous report was adequately expressed compared with GFP-Parkin in the cells we used (Figure S2J). Furthermore, transfection with the TIM23 siRNAs (#a and #b) inhibited mitochondrial localization of YFP-Parkin and reduced PINK1 protein levels (Figures S2K, S2L, and S2M), confirming that severely impaired TIM23 function causes a failure of Parkin recruitment regardless

**Figure 2. TIM23 is crucial for the accumulation and autophosphorylation of PINK1 on damaged mitochondria**

(A) Cells were transfected with siRNA for either luciferase (Luc), PINK1, or TIM23 (#a–#d), treated with or without 10 μM CCCP, and subjected to immunoblot analysis. Open and solid arrowheads denote phosphorylated and unphosphorylated forms of PINK1, respectively. Intensity represents normalized values of band intensity of the corresponding TIM23 protein.

(B–D) Cells expressing GFP-Parkin were transfected with the indicated siRNAs, treated with CCCP, and subjected to analysis of either the intracellular localization of GFP-Parkin (B and C) or immunoblotting with anti-Parkin antibody (D). Ubi represents GFP-Parkin autoubiquitination as an index of its mitochondrial recruitment. Data represent the mean ± SEM of three independent experiments. **$p < 0.0001$ (ANOVA with Tukey's post hoc test).

(E and F) The expression plasmid for wild-type (WT) or kinase-dead PINK1-3HA was introduced into cells transfected with TIM23 siRNA (#a), treated with CCCP, and subjected to analysis of the GFP-Parkin localization. Asterisks indicate transfected cells that were DsRed positive. Data represent the mean ± SEM of three independent experiments. ***$p < 0.0000001$ (Student's t test). Scale bars, 20 μm.

(G) Cells stably expressing PINK1-3HA were transfected with siRNA for Luc or TIM23 (#a), treated with 10 μM CCCP for the indicated times, and subjected to SDS-PAGE with or without Phos-tag and immunoblot analysis.

(H) Mitochondrial fractions were prepared from the cells described in (G), solubilized with digitonin, and analyzed by CN-PAGE and immunoblotting. Mitochondrial fraction prepared from TIM23-KD cells was increased 7-fold to adjust to the protein levels of PINK1-3HA in the control mitochondrial fraction. Open and solid arrowheads indicate phosphorylated and unphosphorylated forms of PINK1, respectively. Ratio (P/U) represents the ratio of band intensity values of the phosphorylated form (P) of PINK1-3HA against the unphosphorylated form (U). Arrow denotes PINK1-3HA-containing protein complex.

See also Figure S2.

of the ectopic fluorescent proteins. The apparent discrepancy with the previous study may be due to different procedures of transfection with TIM23 siRNAs.

To further examine whether the decrease in PINK1 levels was due to the disappearance of TIM23 protein or to functional impairment of the TIM23 complex, the other core subunits were downregulated. We first knocked down the expression of TIM50, which plays an essential role in the mitochondrial import of proteins with a presequence.[25,26] Two TIM50-specific siRNAs induced a more than 92% reduction in its expression (Figure S2N) and led to a strong inhibition of mito-GFP translocation (Figures S2P and S2Q). TIM50 KD, however, caused no obvious reduction in PINK1 protein levels (Figure S2N) or significant changes in PINK1 mRNA levels (Figure S2O). In addition, mitochondrial recruitment of GFP-Parkin was usually observed in the TIM50-KD cells (Figures S2R and S2S). Next, we downregulated TIM17, an integral membrane protein involved in the regulation of TIM23 translocase activity.[27] Because two isoforms (TIM17A and TIM17B) are ubiquitously expressed in human cells,[28] both TIM17 isoforms were knocked down simultaneously. Double knockdown (DKD) of TIM17 A/B resulted in a more than 91% reduction in their protein levels (Figure S2T) and severe impairment of mito-GFP translocation (Figures S2U and S2V). In contrast, PINK1 accumulation and Parkin mitochondrial localization in response to depolarization were not affected by TIM17 A/B DKD (Figures S2T, S2W, and S2X). These findings suggest that loss of TIM23, rather than dysfunction of the TIM23 complex, results in a failure of PINK1 accumulation. Taken together, TIM23 itself is required for PINK1 accumulation and the subsequent Parkin recruitment to depolarized mitochondria.

## TIM23 downregulation significantly delays autophosphorylation of PINK1

To examine whether the decrease in PINK1 levels caused by TIM23 inactivation was solely responsible for the mislocalization of Parkin, wild-type and a kinase-dead mutant of PINK1-3HA were exogenously expressed in TIM23-KD cells carrying GFP-Parkin, followed by CCCP treatment. Ectopic expression of wild-type PINK1, but not the kinase-dead mutant, suppressed the deficiency in the mitochondrial recruitment of GFP-Parkin (Figures 2E and 2F), suggesting that a reduction in the protein levels of active PINK1, not a failure of mitochondrial delivery of other proteins, primarily accounts for the Parkin mislocalization caused by TIM23 downregulation.

In depolarized mitochondria, PINK1 is accumulated on the MOM and autophosphorylated to enhance its kinase activity.[29] Detection of the phosphorylated and unphosphorylated forms of PINK1 in TIM23-KD cells upon treatment with CCCP was equivalent (Figure 2A, TIM23-specific siRNA #a and #b). Therefore, we examined whether TIM23 inactivation affected the phosphorylation status of PINK1. Cells stably expressing PINK1-3HA were transfected with control or TIM23-specific siRNA (#a), treated with CCCP for different incubation times, and analyzed by phosphate-affinity SDS-PAGE (Phos-tag SDS-PAGE). At 2-h incubation with CCCP, the amount of phosphorylated PINK1-3HA (+Phos-tag, open arrowhead) detected was equal to that of its unphosphorylated form (solid arrowhead) in control cells, but the amount of the phosphorylated form was significantly smaller than that of the unphosphorylated form in TIM23-KD cells (Figure 2G). Because PINK1 autophosphorylation tightly couples with the formation of its protein complex,[29] we further analyzed the formation of PINK1 complexes using CN-PAGE. To adjust the protein levels of PINK1-3HA, the mitochondrial fraction prepared from TIM23-KD cells was increased. After 2-h incubation with CCCP, a PINK1-3HA complex in control cells had clearly assembled, whereas the complex in TIM23-KD cells was faintly detected (Figure 2H). These results indicated that TIM23 inactivation delayed PINK1 autophosphorylation. Thus, TIM23 also provides qualitative support for PINK1 activation. Meanwhile, upon prolonged incubation with CCCP, the amount of the PINK1-3HA complex in TIM23-KD cells was roughly equivalent to that in control cells (Figure S2Y), indicating that PINK1 eventually assembles into a protein complex even when TIM23 is repressed. Together, TIM23 downregulation influenced both the accumulation and phosphorylation of PINK1 but not the formation of the PINK1 complex.

## The inner membrane protease OMA1 represses hyperaccumulation of PINK1 in depolarized mitochondria

PINK1 is delivered to mitochondria with the $\Delta\psi m$, processed by PARL, and eventually degraded by proteasomes in the cytoplasm.[7] We therefore examined whether the PINK1 decrease by TIM23 inactivation depended on proteasome activities. TIM23 siRNA-transfected cells were subjected to combined treatment with CCCP and proteasome inhibitors (bortezomib and MG132). In the absence of CCCP, the processed form of PINK1 (red arrowhead) robustly accumulated following treatment with the proteasome inhibitors in both control and TIM23-KD cells (Figure 3A). Upon treatment with CCCP, phosphorylated PINK1 (open arrowhead) was clearly observed in control cells but barely detected in TIM23-KD cells even in the presence of proteasome inhibitors, suggesting that proteasome-mediated cytoplasmic degradation is unnecessary for the decrease in PINK1 levels induced by TIM23 inactivation.

We previously demonstrated that downregulation of the MIM proteins MIC60 and MIC19 interfered with PINK1 accumulation in response to depolarization.[30] TIM23 downregulation, however, did not affect MIC60 and MIC19 protein levels (Figure S3A). To further search for proteins involved in PINK1 accumulation on depolarized mitochondria, we knocked down mitochondrial proteases localized in the intermembrane space and/or MIM. PARL mediates the proteolytic destabilization of PINK1 in energized mitochondria, and mutations in HTRA2 are associated with PD.[6,31] Gene silencing of either PARL or HTRA2, however, did not influence the PINK1 accumulation induced by CCCP treatment (Figure 3B). Although the i-AAA-protease subunit YME1L facilitates PARL-dependent proteolytic processing of PINK1,[32] YME1L downregulation did not affect PINK1 levels in depolarized mitochondria. In contrast, inactivation of the metalloprotease OMA1 led to a clear increase in PINK1 levels upon CCCP treatment, consistent with findings from an earlier study.[24] Downregulation of the m-AAA protease subunit AFG3L2 also increased the PINK1 accumulation in depolarized mitochondria. Interestingly, AFG3L2 downregulation induced not only the disappearance of AFG3L2 but also OMA1 destabilization,

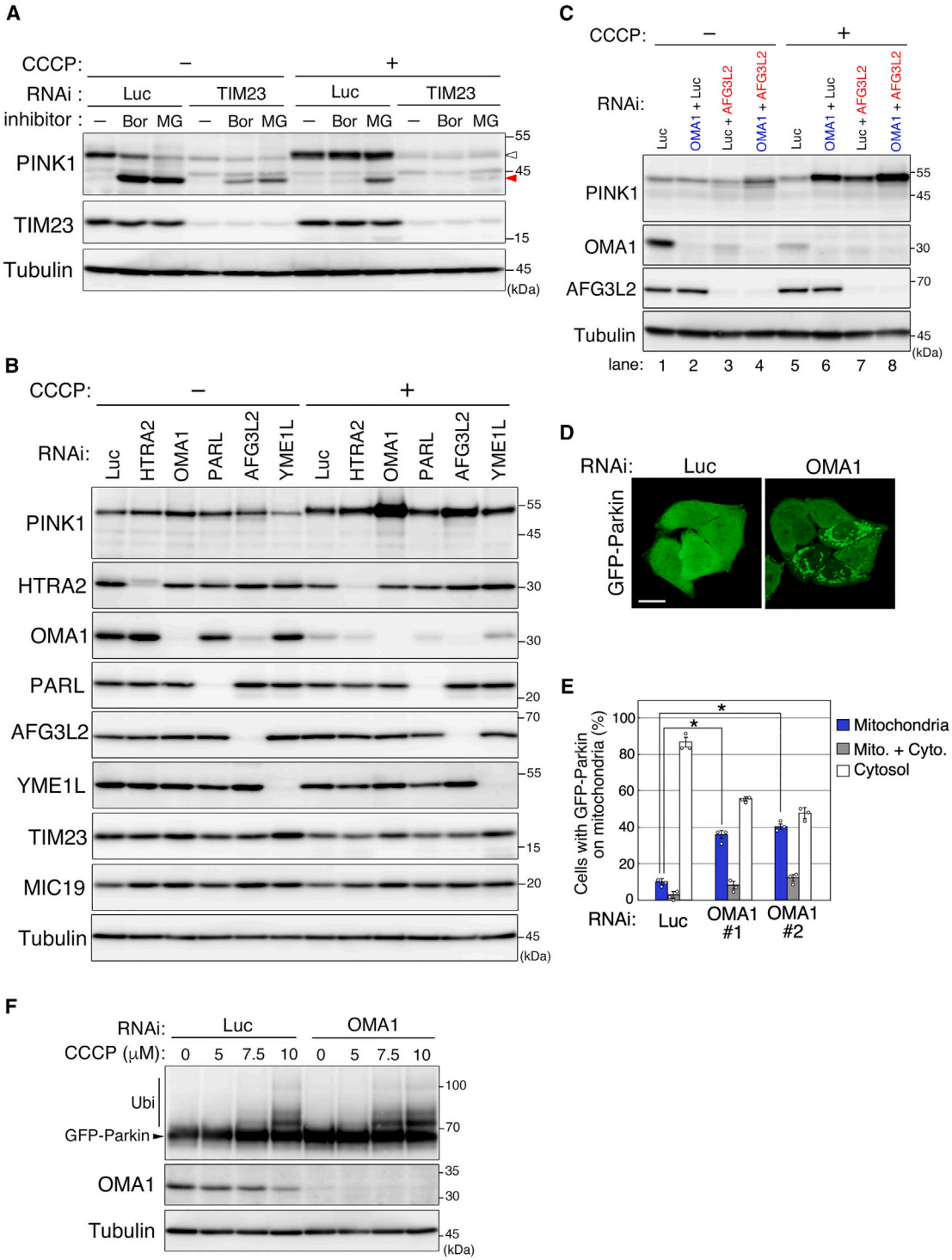


**Figure 3. OMA1 is involved in PINK1 degradation in damaged mitochondria**

(A) Cells transfected with siRNA for Luc or TIM23 (#a) were pretreated with 10 μM CCCP for 30 min, further incubated with 0.5 μM bortezomib (Bor) or 50 μM MG132 (MG) for 4 h, and analyzed by immunoblotting. Open and red arrowheads indicate full-length and processed forms of PINK1, respectively.

(B) Cells were transfected with the indicated siRNA, treated with CCCP, and analyzed by immunoblotting.

(C) Cells were transfected with each possible pair of siRNA for Luc, OMA1, and AFG3L2, treated with CCCP, and analyzed by immunoblotting.

(D–F) Cells expressing GFP-Parkin were transfected with siRNA for OMA1, treated with 7 μM (D and E) or the indicated concentrations of CCCP (F), and subjected to analysis of GFP-Parkin localization (D and E) or immunoblotting with anti-Parkin antibody (F). Scale bar, 20 μm. Data represent the mean ± SEM of three independent experiments. *$p < 0.05$ (ANOVA with Tukey's post hoc test).

See also Figure S3.

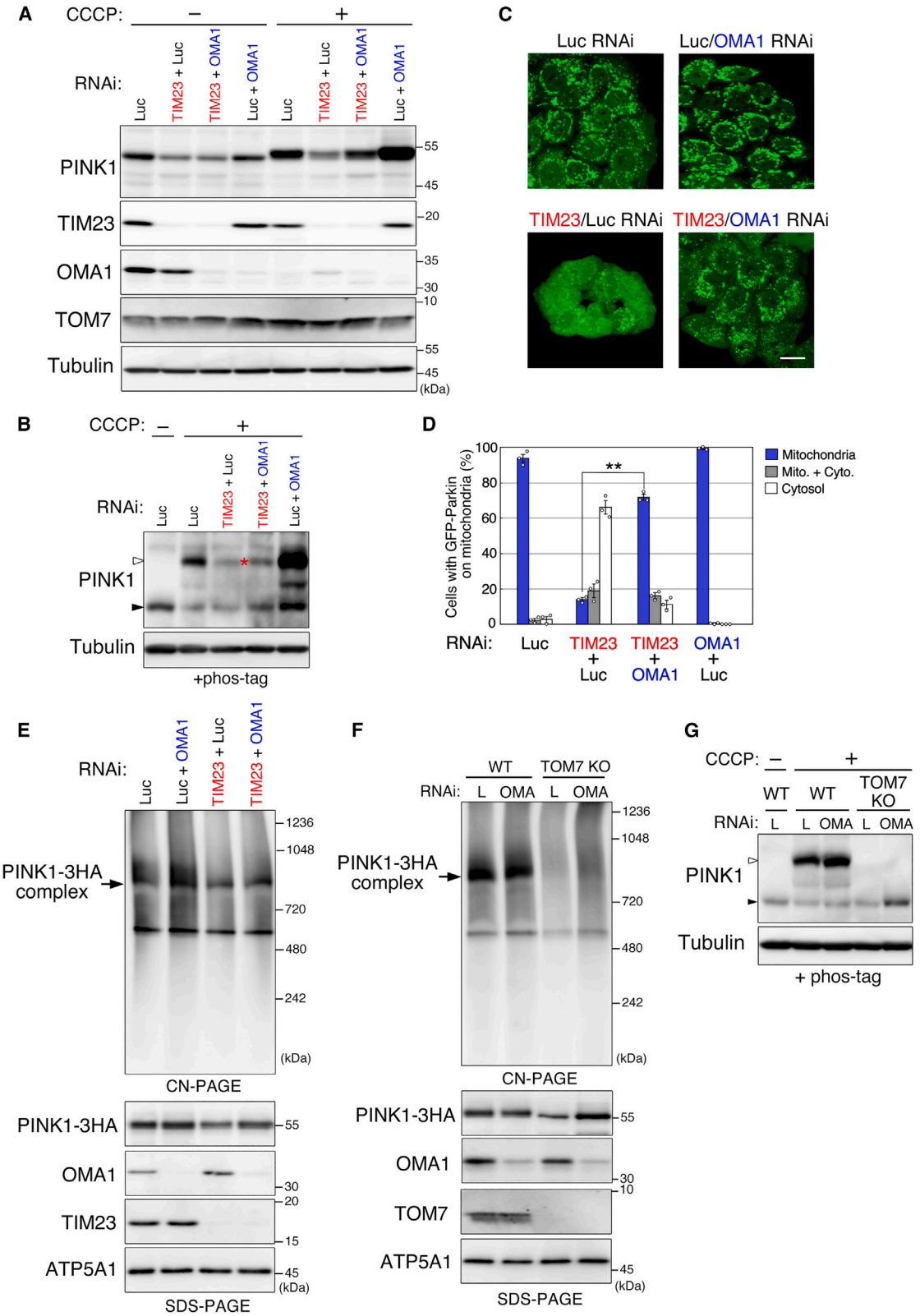


*(legend on next page)*

suggesting that the PINK1 increase caused by AFG3L2 downregulation was primarily due to reduced OMA1 expression. Compared with single inactivation of AFG3L2, however, DKD of OMA1 and AFG3L2 remarkably increased PINK1 levels (Figure 3C, lane 7 vs. lane 8), suggesting that OMA1 destabilization caused by AFG3L2 downregulation is inadequate to increase PINK1 levels. In comparison with OMA1 downregulation, simultaneous inactivation of OMA1 and AFG3L2 induced a slight increase in PINK1 levels (Figure 3C, lane 6 vs. lane 8). Similar results were obtained using another AFG3L2-specific siRNA (Figure S3B). Together, both OMA1 and AFG3L2 were responsible for PINK1 degradation, and OMA1 contributed predominantly to PINK1 destabilization. Notably, a decrease in MIC19 levels was never observed by OMA1 inactivation (Figure 3B), although a significant reduction in MIC19 levels was reported in OMA1-knockout (KO) mouse embryonic fibroblasts.[33] Because OMA1 and YME1L are reciprocally degraded,[34] the prolonged disappearance of OMA1 may lead to the hyperactivation of other proteases, including YME1L, and subsequent degradation in an OMA1-independent manner.

OMA1 downregulation increased PINK1 protein levels on depolarized mitochondria. Transfection with the OMA1 siRNAs, however, did not cause significant changes in PINK1 mRNA levels or an apparent decrease in the $\Delta\psi m$ (Figures S3C and S3D), suggesting that PINK1 accumulation is due to the deficiency of OMA1-mediated degradation. We next examined whether PINK1 accumulated by OMA1 inactivation was active and enhanced Parkin recruitment to depolarized mitochondria. Cells stably expressing GFP-Parkin were transfected with OMA1-specific siRNA and incubated with 7 μM CCCP, an amount that is usually inadequate to induce an apparent recruitment of GFP-Parkin. After 90-min incubation with CCCP, cytosolic localization of GFP-Parkin was still observed in most of the control cells, whereas a significant number of cells (36%–40%) exhibited mitochondrial localization of GFP-Parkin upon OMA1 inactivation (Figures 3D and 3E). Moreover, upon treatment with 7.5 μM CCCP, autoubiquitination of GFP-Parkin was robustly detected in OMA1-KD cells but not in control cells (Figure 3F). These findings indicated that OMA1 downregulation stimulated Parkin recruitment through an increase in PINK levels and suggested that OMA1 played a critical role in preventing an excessive accumulation of active PINK1 by mitochondrial depolarization.

## OMA1 is responsible for PINK1 degradation and Parkin mislocalization caused by TIM23 downregulation

To examine whether PINK1 reduction caused by TIM23 downregulation depended on OMA1, we simultaneously knocked down TIM23 and OMA1. Without CCCP, a reduction in PINK1 levels was still observed, even in TIM23/OMA1-DKD cells. In the presence of CCCP, PINK1 levels were clearly recovered by DKD of TIM23 and OMA1, compared with TIM23 KD (Figure 4A). Analysis using Phos-tag SDS-PAGE revealed that PINK1 recovered by TIM23/OMA1 DKD was robustly phosphorylated (Figure 4B, asterisk), indicating that OMA1 inactivation leads to the recovery of active PINK1 in response to depolarization. Similar results were obtained using another OMA1-specific siRNA (Figures S3E and S3F). Moreover, the deficiency in Parkin recruitment caused by TIM23 downregulation was significantly suppressed by additive inactivation of OMA1 (Figures 4C and 4D). Treatment with proteasome inhibitors did not enhance the recovery of PINK1 levels induced by OMA1 inactivation (Figures S3H and S3I), confirming the dispensability of proteasomes. These findings indicated that OMA1 was responsible for PINK1 degradation and Parkin mislocalization caused by TIM23 downregulation.

We also investigated the effects of other mitochondrial proteases on PINK1 degradation caused by TIM23 inactivation. Downregulation of neither PARL nor YME1L influenced the PINK1 decrease in TIM23-KD cells, regardless of CCCP (Figures S3L and S3M). As expected, AFG3L2 inactivation in TIM23-KD cells induced an increase in PINK1 levels upon CCCP treatment (Figure S3J). Interestingly, PINK1 reduction caused by TIM23 downregulation was also suppressed by additive inactivation of HTRA2 (Figure S3K), despite the fact that inactivation of HTRA2 alone did not affect PINK1 accumulation (Figure 3B). A similar result was observed using another HTRA2-specific siRNA. The results suggest that HTRA2 does not usually contribute to PINK1 degradation but may be enzymatically activated by the loss of TIM23. Overall, AFG3L2 and HTRA2, in addition to OMA1, are directly and/or indirectly involved in PINK1 degradation caused by TIM23 downregulation.

## TIM23 plays a distinct role in PINK1 activation independently of TOM7

Ablation of TOM7, a subunit of the TOM complex, leads to a decrease in PINK1 levels that is suppressed by OMA1 inactivation (Figure S4A).[24] To address the possibility that the decrease in PINK1 levels by TIM23 downregulation was due primarily to a loss of TOM7, we quantified TOM7 levels when TIM23 expression was repressed. In addition to immunoblot analysis, parallel reaction monitoring (PRM), an MS/MS-based targeted quantification method, was applied to measure TOM7 levels as it is more suitable for quantifying a small and mostly hydrophobic

**Figure 4. OMA1 inactivation restored the deficiencies in PINK1 accumulation and Parkin recruitment induced by TIM23 downregulation**

(A and B) Cells transfected with each possible pair of siRNA for Luc, OMA1, and TIM23 (#a) were treated with CCCP, subjected to SDS-PAGE (A) or Phos-tag SDS-PAGE (B), and analyzed by immunoblotting. Asterisk represents the phosphorylated form of PINK1 in TIM23/OMA1-DKD cells.

(C and D) Cells expressing GFP-Parkin were treated as described in (A) and subjected to analysis of GFP-Parkin localization. Data represent the mean ± SEM of three independent experiments. $^{**}p < 0.005$ (ANOVA with Tukey's post hoc test). Scale bar, 20 μm.

(E) Mitochondrial fractions were prepared from cells treated as described in (A), digitonin-solubilized, and subjected to SDS-PAGE or CN-PAGE followed by immunoblotting.

(F and G) Digitonin-solubilized mitochondrial fractions prepared from control (WT) and TOM7-KO cells transfected with siRNA for Luc (L) or OMA1 (OMA) were subjected to CN-PAGE (F) or Phos-tag SDS-PAGE (G), followed by immunoblotting. Open and solid arrowheads indicate the phosphorylated and unphosphorylated forms of PINK1, respectively. Arrow denotes PINK1-3HA-containing protein complex.

See also Figure S4.

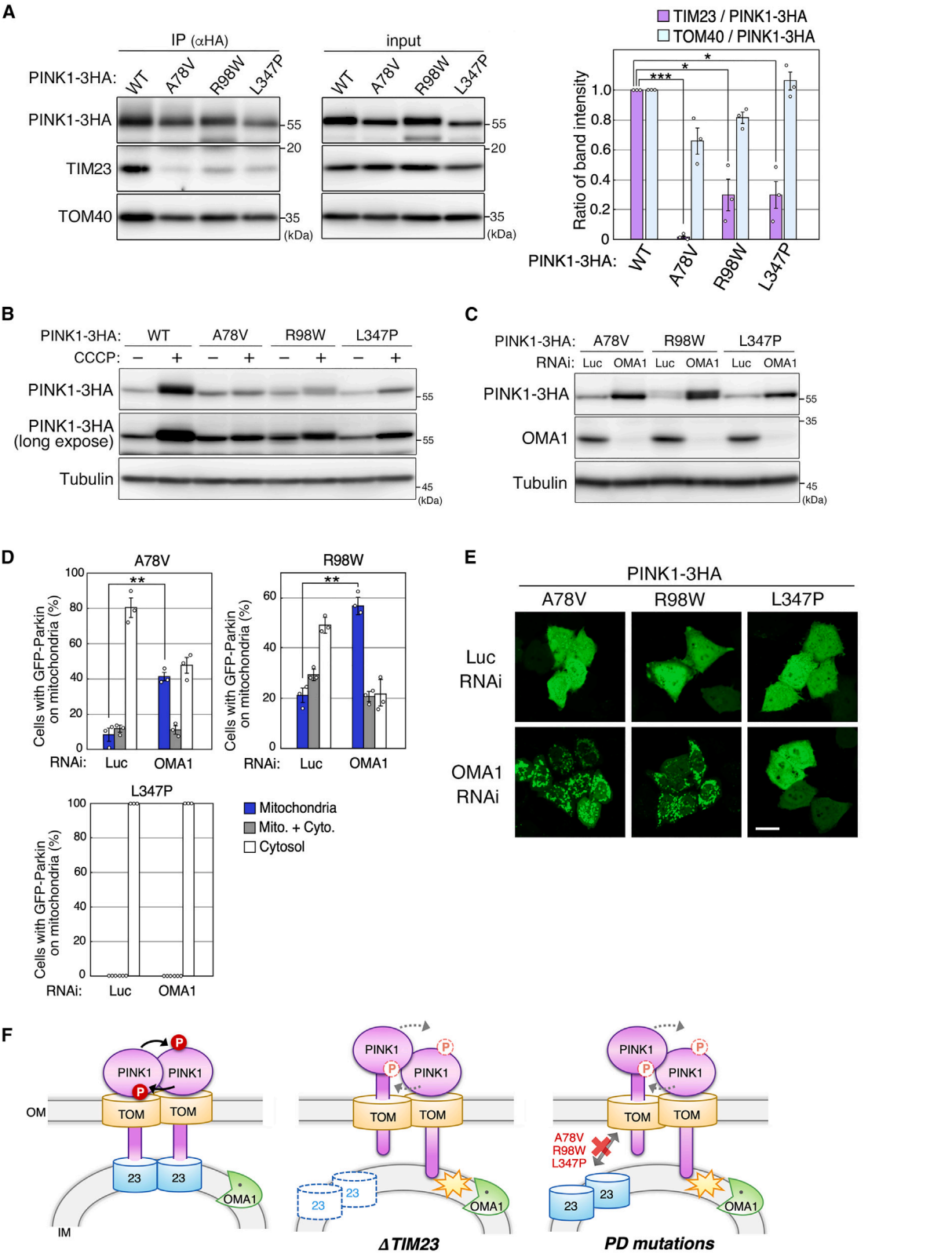


*(legend on next page)*

protein. PRM analysis showed that steady-state protein levels of TOM7 remained mostly unchanged irrespective of TIM23 (Figure S3G). Furthermore, TIM23 levels were also unaltered even upon TOM7 ablation (Figure S4A). These findings indicated that TIM23 and TOM7 were separately required for PINK1 accumulation on depolarized mitochondria.

PINK1 recovered by OMA1 inactivation in TIM23-KD cells enabled Parkin to be recruited to depolarized mitochondria (Figures 4C and 4D), whereas PINK1 restored by OMA1 inactivation in TOM7-KO cells fails to induce Parkin recruitment.[24] To further investigate functional differences in these PINK1 proteins recovered by OMA1 inactivation, the formation of the PINK1 complex was analyzed by CN-PAGE. Mitochondrial fractions prepared from cells expressing PINK1-3HA were utilized because of the reduction in endogenous PINK1 levels caused by downregulation of TIM23 or TOM7. As expected, assembly of the PINK1 complex was observed upon TIM23 and OMA1 inactivation (Figure 4E), consistent with the phosphorylation status of PINK1 in TIM23/OMA1-DKD cells (Figure 4B). On the other hand, PINK1 prepared from TOM7-KO cells failed to form a protein complex regardless of OMA1 (Figure 4F). Consistently, analysis using Phos-tag SDS-PAGE showed that PINK1 remained unphosphorylated in TOM7-KO cells irrespective of OMA1 (Figure 4G). Similar results were obtained by analysis of endogenous PINK1 protein (Figures S4B and S4C). These results strongly indicated that TIM23 had a distinct function in PINK1 activation independent of TOM7 function.

### OMA1 facilitates the degradation of pathogenic PINK1 mutants that fail to interact with TIM23

To investigate the pathophysiological aspects of the association with TIM23, we searched for pathogenic PINK1 mutations that disrupt or weaken the interaction with TIM23 by immunoprecipitation of PINK1-3HA (Figure S5A). Among 24 mutations in the PINK1 gene, three of the pathogenic variants (A78V, R98W, and L347P) barely co-precipitated with TIM23, but they were significantly associated with TOM40 (Figure 5A). Immunofluorescence analysis showed that three PINK1 mutants were normally transported into depolarized mitochondria (Figure S5B). Localization of a PINK1 (R98W) mutant in energized mitochondria was confirmed because it is insensitive to PARL-proteolytic cleavage and eventually imported into the matrix of mitochondria with the $\Delta\psi m$.[6,35] These observations suggest that impaired association of these PINK1 mutants with TIM23 is not due to their mislocalization but rather to the failure of a specific interaction with TIM23. These PINK1 mutants exhibited lower expression even upon CCCP treatment (Figure 5B), and OMA1 inactivation induced an increase in their protein levels (Figure 5C). Furthermore, OMA1 downregulation significantly stimulated the mitochondrial localization of GFP-Parkin in PINK1-KO cells expressing either of two PINK1 mutants (A78V and R98W) (Figures 5D and 5E). PINK1(L347P)-mutant-dependent recruitment of Parkin was not observed because its recombinant mutant protein completely loses the kinase activity.[36] Taken together, OMA1 inactivation increased the expression of PINK1 mutants that barely interacted with TIM23 and consequently stimulated the mitochondrial localization of Parkin, suggesting that OMA1 facilitates selective degradation of pathogenic PINK1 variants dissociated from TIM23.

## DISCUSSION

PINK1 assembles together with the TOM complex into a protein complex with a high molecular weight on native PAGE.[8,9] Other components of PINK1 complexes besides TOM complex subunits, however, have remained unidentified. Using LC-MS/MS analyses and a NAMOS assay, we identified MIM protein TIM23 as a member of the PINK1-containing protein complex. Complex assembly of PINK1 with the TOM complex occurs in the MOM.[8,9] Interactions with TIM23 present in the MIM allow the PINK1 complex to preferentially localize to a contact site between the outer and inner boundary membranes, which is supported by reports that PINK1 interacts with MIC60 and SAM50, components of the mitochondrial intermembrane space-bridging complex present at the contact site.[30,37] Exogenously overexpressed PINK1 is utilized in numerous studies because of the low expression of endogenous PINK1, giving rise to concerns about the indirect effects of excess amounts of PINK1. In most of our experiments, we quantified endogenous PINK1 using monoclonal antibodies that specifically recognize the protein even without uncouplers and demonstrated that TIM23 facilitates the accumulation of PINK1 on the MOM in response to mitochondrial depolarization. This finding is consistent with a previous report that a lipopeptide produced by the fungi *Streptomyces* inhibits TIM23-mediated protein translocation and attenuates PINK1 accumulation upon treatment with the uncoupler.[38] Furthermore, we discovered three pathogenic PINK1 mutations (A78V, R98W, and L347P) that disrupt interactions between PINK1 and TIM23. The L347P mutation is considered to indirectly affect TIM23 association through conformational changes because it is found in the cytosolic kinase domain. Two other mutations (A78V and R98W) are mapped to a segment facing the intermembrane space and transmembrane domain of

**Figure 5. Analysis of pathogenic PINK1 variants that fail to interact with TIM23**

(A) Cells transfected with expression plasmids carrying wild-type (WT) or the indicated pathogenic variants of PINK1-3HA were treated with CCCP, immunoprecipitated with an anti-HA antibody, and subjected to immunoblot analysis. Input, 3% of solubilized cell lysates. Data represent the mean ± SEM of three independent experiments. *$p < 0.05$, ***$p < 0.0001$ (ANOVA with Dunnett's post hoc test).

(B) Cells were treated as described in (A) and subjected to immunoblotting analysis.

(C) Cells expressing the indicated pathogenic variants of PINK1-3HA were transfected with siRNA for OMA1, treated with CCCP, and analyzed by immunoblotting.

(D and E) PINK1-KO cells were co-transfected with GFP-Parkin and the indicated pathogenic variants of PINK1-3HA, treated with 7 μM CCCP, and subjected to analysis of GFP-Parkin localization. Data represent the mean ± SEM of three independent experiments. **$p < 0.005$ (Student's t test). Scale bar, 20 μm.

(F) Schematic model of TIM23 for safeguarding PINK1. See discussion for description.

See also Figure S5.

PINK1, respectively. These regions carrying the mutations differ from the mitochondrial targeting sequence (MTS), and the PINK1 variants were normally translocated to depolarized mitochondria, suggesting that the MTS of the PINK1 variants retains the ability to interact with at least the TOM complex. Thus, the pathogenic mutations would not interfere with targeting to the mitochondria but rather with the subsequent association with TIM23 in depolarized mitochondria.

Investigations of TIM23 function to date were performed only using energized mitochondria, due to the requirement of the $\Delta\psi m$ for TIM23-mediated protein translocation.[16–18] Our results revealed TIM23-dependent PINK1 stabilization and OMA1-mediated PINK1 degradation in depolarized mitochondria, suggesting that TIM23 protects PINK1 from OMA1 activated by the $\Delta\psi m$ loss. OPA1, an MIM protein that facilitates fusion between MIMs, is a well-characterized substrate for stress-induced processing by OMA1 and is proteolytically cleaved to interrupt membrane fusion during dissipation of the $\Delta\psi m$.[39,40] Unlike OPA1, PINK1 must be stabilized in depolarized mitochondria where OMA1 is activated. Therefore, TIM23 would be present in the PINK1 complex to sequester PINK1 from stress-activated proteases including OMA1 (Figure 5F), despite not participating directly in assembling the PINK1 complex. The pathogenic mutations found in this study weakened the interactions between PINK1 and TIM23. Consequently, OMA1-dependent degradation of the PINK1 mutants in depolarized mitochondria would be accelerated (PD mutations in Figure 5F). Crystal structure analyses suggest that autophosphorylation at Ser228 of human PINK1 occurs in *trans* in a protein complex containing two PINK1 molecules.[41,42] Together with our finding that TIM23 inactivation significantly delays the autophosphorylation of PINK1, attenuation of PINK1 phosphorylation by TIM23 downregulation may result from misalignment in a vertical direction between PINK1 molecules present in a protein complex (ΔTIM23 in Figure 5F). Thus, in addition to safeguarding PINK1, TIM23 may ensure the correct position for efficient *trans* autophosphorylation.

OMA1 is an MIM protease that governs stress-induced degradation of a variety of MIM proteins including OPA1, YME1L, DELE1, and respiratory chain subunits.[34,39,40,43–45] OMA1 also controls PINK1 degradation upon TOM7 ablation.[24] Combined with our finding that a loss of TOM7 caused a failure of assembly of the PINK1 complex, unassembled PINK1 appears to be a substrate for degradation by OMA1. Furthermore, OMA1 inactivation stimulated PINK1 accumulation in depolarized mitochondria, indicating that PINK1 is usually degraded by OMA1 irrespective of TOM7. Taken together, these findings suggest that OMA1 prevents PINK1 from being hyperaccumulated by the rapid removal of PINK1 disassociated from the protein complex, and TIM23 might determine the maximum amount of the PINK1 complex by protecting assembled PINK1.

In energized mitochondria, PINK1 targets the TOM complex, reaches to the TIM23 complex, is cleaved by PARL, and is then degraded by cytoplasmic proteasomes.[6,7] In addition to proteasomes, our results indicated that OMA1, in cooperation with AFG3L2, promoted PINK1 degradation in energized mitochondria. In active mitochondria, a large number of mitochondrial precursors pass through the TIM23 complex, leading to a consecutive occupation of TIM23 by the precursors. Consequently, PINK1 would be kept away from the TIM23 complex and barely subjected to PARL cleavage. Thus, in the mitochondria where translocation via the TIM23 complex consecutively occurs, OMA1/AFG3L2, rather than PARL, may contribute to the rapid removal of PINK1 and prevent unnecessary initiation of mitochondrial elimination. The discovery of TIM23 in PINK1 protein complexes illuminates another aspect of the mitochondrial translocase and has begun to unveil its $\Delta\psi m$-independent role in the activation of mitochondrial autophagy, providing a clue to understanding the regulation of mitochondrial surveillance through PINK1 proteostasis mediated by mitochondrial proteases.

### Limitations of the study

Our strategy of gene silencing using RNA interference techniques for investigating the functions of TIM23, which is indispensable for cell growth, may limit interpretations as a consequence of indirect effects of the compromised translocase activity. In addition to immunoprecipitation techniques, complex purification and *in vitro* reconstitution would be necessary for determining the stoichiometry of the PINK complexes and elucidating the physiological interactions of PINK1 and TIM23. Further studies will help to validate alternative roles of TIM23 in mitochondrial surveillance.

## STAR★METHODS

Detailed methods are provided in the online version of this paper and include the following:

- KEY RESOURCES TABLE
- RESOURCE AVAILABILITY
  - Lead contact
  - Materials availability
  - Data and code availability
- EXPERIMENTAL MODEL AND SUBJECT DETAILS
  - Cell lines
- METHOD DETAILS
  - Vital staining of mitochondria
  - Analysis of Parkin intracellular localization
  - DNA and siRNA transfection
  - RNA preparation and quantitative PCR
  - Immunoblot
  - Clear native PAGE
  - Immunoprecipitation
  - LC-MS/MS analysis
- QUANTIFICATIONS AND STATISTICAL ANALYSIS

### SUPPLEMENTAL INFORMATION

Supplemental information can be found online at https://doi.org/10.1016/j.celrep.2023.112454.

### ACKNOWLEDGMENTS

We greatly appreciate Richard J. Youle for providing the TOM7-KO- and YFP-Parkin-expressing cells. We thank Hiromi Hirose and Tomie Kameyama for excellent technical assistance. This work was supported by Grants-in-Aid

for Scientific Research from the Japan Society for the Promotion of Science (grant number 20H03257 to T.O.), the Japan Agency for Medical Research and Development (grant numbers JP21gm1410002 and JP22gm1410002 to T.O.), and Joint Usage and Joint Research Programs by the Institute of Advanced Medical Sciences of Tokushima University.

## AUTHOR CONTRIBUTIONS

S.A., K.W., K.N., S.-i.Y., H.K., M.K., and T.O. performed experiments and analyzed the data. S.A., H.K., S.S., T.K., N.M., T.E., and T.O. contributed to preparing the manuscript.

## DECLARATION OF INTERESTS

The authors declare no competing interests.

Received: June 29, 2022
Revised: February 24, 2023
Accepted: April 16, 2023
Published: May 8, 2023

## REFERENCES

1. Bandres-Ciga, S., Diez-Fairen, M., Kim, J.J., and Singleton, A.B. (2020). Genetics of Parkinson's disease: an introspection of its journey towards precision medicine. Neurobiol. Dis. *137*, 104782. https://doi.org/10.1016/j.nbd.2020.104782.
2. Day, J.O., and Mullin, S. (2021). The genetics of Parkinson's disease and implications for clinical practice. Genes *12*, 1006. https://doi.org/10.3390/genes12071006.
3. Pickrell, A.M., and Youle, R.J. (2015). The roles of PINK1, parkin, and mitochondrial fidelity in Parkinson's disease. Neuron *85*, 257–273. https://doi.org/10.1016/j.neuron.2014.12.007.
4. Agarwal, S., and Muqit, M.M.K. (2022). PTEN-induced kinase 1 (PINK1) and Parkin: unlocking a mitochondrial quality control pathway linked to Parkinson's disease. Curr. Opin. Neurobiol. *72*, 111–119. https://doi.org/10.1016/j.conb.2021.09.005.
5. Sekine, S. (2020). PINK1 import regulation at a crossroad of mitochondrial fate: the molecular mechanisms of PINK1 import. J. Biochem. *167*, 217–224. https://doi.org/10.1093/jb/mvz069.
6. Jin, S.M., Lazarou, M., Wang, C., Kane, L.A., Narendra, D.P., and Youle, R.J. (2010). Mitochondrial membrane potential regulates PINK1 import and proteolytic destabilization by PARL. J. Cell Biol. *191*, 933–942. https://doi.org/10.1083/jcb.201008084.
7. Yamano, K., and Youle, R.J. (2013). PINK1 is degraded through the N-end rule pathway. Autophagy *9*, 1758–1769. https://doi.org/10.4161/auto.24633.
8. Lazarou, M., Jin, S.M., Kane, L.A., and Youle, R.J. (2012). Role of PINK1 binding to the TOM complex and alternate intracellular membranes in recruitment and activation of the E3 ligase Parkin. Dev. Cell *22*, 320–333. https://doi.org/10.1016/j.devcel.2011.12.014.
9. Okatsu, K., Uno, M., Koyano, F., Go, E., Kimura, M., Oka, T., Tanaka, K., and Matsuda, N. (2013). A dimeric PINK1-containing complex on depolarized mitochondria stimulates Parkin recruitment. J. Biol. Chem. *288*, 36372–36384. https://doi.org/10.1074/jbc.M113.509653.
10. Okatsu, K., Oka, T., Iguchi, M., Imamura, K., Kosako, H., Tani, N., Kimura, M., Go, E., Koyano, F., Funayama, M., et al. (2012). PINK1 autophosphorylation upon membrane potential dissipation is essential for Parkin recruitment to damaged mitochondria. Nat. Commun. *3*, 1016. https://doi.org/10.1038/ncomms2016.
11. Koyano, F., Okatsu, K., Kosako, H., Tamura, Y., Go, E., Kimura, M., Kimura, Y., Tsuchiya, H., Yoshihara, H., Hirokawa, T., et al. (2014). Ubiquitin is phosphorylated by PINK1 to activate parkin. Nature *510*, 162–166. https://doi.org/10.1038/nature13392.
12. Kane, L.A., Lazarou, M., Fogel, A.I., Li, Y., Yamano, K., Sarraf, S.A., Banerjee, S., and Youle, R.J. (2014). PINK1 phosphorylates ubiquitin to activate Parkin E3 ubiquitin ligase activity. J. Cell Biol. *205*, 143–153. https://doi.org/10.1083/jcb.201402104.
13. Ordureau, A., Sarraf, S.A., Duda, D.M., Heo, J.M., Jedrychowski, M.P., Sviderskiy, V.O., Olszewski, J.L., Koerber, J.T., Xie, T., Beausoleil, S.A., et al. (2014). Quantitative proteomics reveal a feedforward mechanism for mitochondrial PARKIN translocation and ubiquitin chain synthesis. Mol. Cell *56*, 360–375. https://doi.org/10.1016/j.molcel.2014.09.007.
14. Heo, J.M., Ordureau, A., Paulo, J.A., Rinehart, J., and Harper, J.W. (2015). The PINK1-PARKIN mitochondrial ubiquitylation pathway drives a program of OPTN/NDP52 recruitment and TBK1 activation to promote mitophagy. Mol. Cell *60*, 7–20. https://doi.org/10.1016/j.molcel.2015.08.016.
15. Lazarou, M., Sliter, D.A., Kane, L.A., Sarraf, S.A., Wang, C., Burman, J.L., Sideris, D.P., Fogel, A.I., and Youle, R.J. (2015). The ubiquitin kinase PINK1 recruits autophagy receptors to induce mitophagy. Nature *524*, 309–314. https://doi.org/10.1038/nature14893.
16. Mokranjac, D., and Neupert, W. (2010). The many faces of the mitochondrial TIM23 complex. Biochim. Biophys. Acta *1797*, 1045–1054. https://doi.org/10.1016/j.bbabio.2010.01.026.
17. van der Laan, M., Hutu, D.P., and Rehling, P. (2010). On the mechanism of preprotein import by the mitochondrial presequence translocase. Biochim. Biophys. Acta *1803*, 732–739. https://doi.org/10.1016/j.bbamcr.2010.01.013.
18. Horvath, S.E., Rampelt, H., Oeljeklaus, S., Warscheid, B., van der Laan, M., and Pfanner, N. (2015). Role of membrane contact sites in protein import into mitochondria. Protein Sci. *24*, 277–297. https://doi.org/10.1002/pro.2625.
19. van der Laan, M., Wiedemann, N., Mick, D.U., Guiard, B., Rehling, P., and Pfanner, N. (2006). A role for Tim21 in membrane-potential-dependent preprotein sorting in mitochondria. Curr. Biol. *16*, 2271–2276. https://doi.org/10.1016/j.cub.2006.10.025.
20. Emtage, J.L., and Jensen, R.E. (1993). MAS6 encodes an essential inner membrane component of the yeast mitochondrial protein import pathway. J. Cell Biol. *122*, 1003–1012. https://doi.org/10.1083/jcb.122.5.1003.
21. Bult, C.J., Blake, J.A., Smith, C.L., Kadin, J.A., and Richardson, J.E.; Mouse Genome Database Group (2019). Mouse genome database (MGD) 2019. Nucleic Acids Res. *47*, D801–D806. https://doi.org/10.1093/nar/gky1056.
22. Narendra, D.P., Jin, S.M., Tanaka, A., Suen, D.F., Gautier, C.A., Shen, J., Cookson, M.R., and Youle, R.J. (2010). PINK1 is selectively stabilized on impaired mitochondria to activate Parkin. PLoS Biol. *8*, e1000298. https://doi.org/10.1371/journal.pbio.1000298.
23. Matsuda, N., Sato, S., Shiba, K., Okatsu, K., Saisho, K., Gautier, C.A., Sou, Y.S., Saiki, S., Kawajiri, S., Sato, F., et al. (2010). PINK1 stabilized by mitochondrial depolarization recruits Parkin to damaged mitochondria and activates latent Parkin for mitophagy. J. Cell Biol. *189*, 211–221. https://doi.org/10.1083/jcb.200910140.
24. Sekine, S., Wang, C., Sideris, D.P., Bunker, E., Zhang, Z., and Youle, R.J. (2019). Reciprocal roles of Tom7 and OMA1 during mitochondrial import and activation of PINK1. Mol. Cell *73*, 1028–1043.e5. https://doi.org/10.1016/j.molcel.2019.01.002.
25. Yamamoto, H., Esaki, M., Kanamori, T., Tamura, Y., Nishikawa, S.i., and Endo, T. (2002). Tim50 is a subunit of the TIM23 complex that links protein translocation across the outer and inner mitochondrial membranes. Cell *111*, 519–528. https://doi.org/10.1016/s0092-8674(02)01053-x.
26. Geissler, A., Chacinska, A., Truscott, K.N., Wiedemann, N., Brandner, K., Sickmann, A., Meyer, H.E., Meisinger, C., Pfanner, N., and Rehling, P. (2002). The mitochondrial presequence translocase: an essential role of Tim50 in directing preproteins to the import channel. Cell *111*, 507–518. https://doi.org/10.1016/s0092-8674(02)01073-5.

27. Martinez-Caballero, S., Grigoriev, S.M., Herrmann, J.M., Campo, M.L., and Kinnally, K.W. (2007). Tim17p regulates the twin pore structure and voltage gating of the mitochondrial protein import complex TIM23. J. Biol. Chem. *282*, 3584–3593. https://doi.org/10.1074/jbc.M607551200.

28. Bauer, M.F., Gempel, K., Reichert, A.S., Rappold, G.A., Lichtner, P., Gerbitz, K.D., Neupert, W., Brunner, M., and Hofmann, S. (1999). Genetic and structural characterization of the human mitochondrial inner membrane translocase. J. Mol. Biol. *289*, 69–82. https://doi.org/10.1006/jmbi.1999.2751.

29. Sekine, S., and Youle, R.J. (2018). PINK1 import regulation; a fine system to convey mitochondrial stress to the cytosol. BMC Biol. *16*, 2. https://doi.org/10.1186/s12915-017-0470-7.

30. Akabane, S., Uno, M., Tani, N., Shimazaki, S., Ebara, N., Kato, H., Kosako, H., and Oka, T. (2016). PKA regulates PINK1 stability and parkin recruitment to damaged mitochondria through phosphorylation of MIC60. Mol. Cell *62*, 371–384. https://doi.org/10.1016/j.molcel.2016.03.037.

31. Vande Walle, L., Lamkanfi, M., and Vandenabeele, P. (2008). The mitochondrial serine protease HtrA2/Omi: an overview. Cell Death Differ. *15*, 453–460. https://doi.org/10.1038/sj.cdd.4402291.

32. Wai, T., Saita, S., Nolte, H., Müller, S., König, T., Richter-Dennerlein, R., Sprenger, H.G., Madrenas, J., Mühlmeister, M., Brandt, U., et al. (2016). The membrane scaffold SLP2 anchors a proteolytic hub in mitochondria containing PARL and the i-AAA protease YME1L. EMBO Rep. *17*, 1844–1856. https://doi.org/10.15252/embr.201642698.

33. Viana, M.P., Levytskyy, R.M., Anand, R., Reichert, A.S., and Khalimonchuk, O. (2021). Protease OMA1 modulates mitochondrial bioenergetics and ultrastructure through dynamic association with MICOS complex. iScience *24*, 102119. https://doi.org/10.1016/j.isci.2021.102119.

34. Rainbolt, T.K., Saunders, J.M., and Wiseman, R.L. (2015). YME1L degradation reduces mitochondrial proteolytic capacity during oxidative stress. EMBO Rep. *16*, 97–106. https://doi.org/10.15252/embr.201438976.

35. Meissner, C., Lorenz, H., Hehn, B., and Lemberg, M.K. (2015). Intramembrane protease PARL defines a negative regulator of PINK1- and PARK2/Parkin-dependent mitophagy. Autophagy *11*, 1484–1498. https://doi.org/10.1080/15548627.2015.1063763.

36. Woodroof, H.I., Pogson, J.H., Begley, M., Cantley, L.C., Deak, M., Campbell, D.G., van Aalten, D.M.F., Whitworth, A.J., Alessi, D.R., and Muqit, M.M.K. (2011). Discovery of catalytically active orthologues of the Parkinson's disease kinase PINK1: analysis of substrate specificity and impact of mutations. Open Biol. *1*, 110012. https://doi.org/10.1098/rsob.110012.

37. Jian, F., Chen, D., Chen, L., Yan, C., Lu, B., Zhu, Y., Chen, S., Shi, A., Chan, D.C., and Song, Z. (2018). Sam50 regulates PINK1-parkin-mediated mitophagy by controlling PINK1 stability and mitochondrial morphology. Cell Rep. *23*, 2989–3005. https://doi.org/10.1016/j.celrep.2018.05.015.

38. Filipuzzi, I., Steffen, J., Germain, M., Goepfert, L., Conti, M.A., Potting, C., Cerino, R., Pfeifer, M., Krastel, P., Hoepfner, D., et al. (2017). Stendomycin selectively inhibits TIM23-dependent mitochondrial protein import. Nat. Chem. Biol. *13*, 1239–1244. https://doi.org/10.1038/nchembio.2493.

39. McBride, H., and Soubannier, V. (2010). Mitochondrial function: OMA1 and OPA1, the grandmasters of mitochondrial health. Curr. Biol. *20*, R274–R276. https://doi.org/10.1016/j.cub.2010.02.011.

40. MacVicar, T., and Langer, T. (2016). OPA1 processing in cell death and disease - the long and short of it. J. Cell Sci. *129*, 2297–2306. https://doi.org/10.1242/jcs.159186.

41. Gan, Z.Y., Callegari, S., Cobbold, S.A., Cotton, T.R., Mlodzianoski, M.J., Schubert, A.F., Geoghegan, N.D., Rogers, K.L., Leis, A., Dewson, G., et al. (2022). Activation mechanism of PINK1. Nature *602*, 328–335. https://doi.org/10.1038/s41586-021-04340-2.

42. Rasool, S., Veyron, S., Soya, N., Eldeeb, M.A., Lukacs, G.L., Fon, E.A., and Trempe, J.F. (2022). Mechanism of PINK1 activation by autophosphorylation and insights into assembly on the TOM complex. Mol. Cell *82*, 44–59.e6. https://doi.org/10.1016/j.molcel.2021.11.012.

43. Wu, Z., Zuo, M., Zeng, L., Cui, K., Liu, B., Yan, C., Chen, L., Dong, J., Shangguan, F., Hu, W., et al. (2021). OMA1 reprograms metabolism under hypoxia to promote colorectal cancer development. EMBO Rep. *22*, e50827. https://doi.org/10.15252/embr.202050827.

44. Scheller, K., Sekeris, C.E., Krohne, G., Hock, R., Hansen, I.A., and Scheer, U. (2000). Localization of glucocorticoid hormone receptors in mitochondria of human cells. Eur. J. Cell Biol. *79*, 299–307. https://doi.org/10.1078/S0171-9335(04)70033-3.

45. Guo, X., Aviles, G., Liu, Y., Tian, R., Unger, B.A., Lin, Y.H.T., Wiita, A.P., Xu, K., Correia, M.A., and Kampmann, M. (2020). Mitochondrial stress is relayed to the cytosol by an OMA1-DELE1-HRI pathway. Nature *579*, 427–432. https://doi.org/10.1038/s41586-020-2078-2.

46. Ishihara, N., and Mihara, K. (1998). Identification of the protein import components of the rat mitochondrial inner membrane, rTIM17, rTIM23, and rTIM44. J. Biochem. *123*, 722–732.

47. Narendra, D., Tanaka, A., Suen, D.F., and Youle, R.J. (2008). Parkin is recruited selectively to impaired mitochondria and promotes their autophagy. J. Cell Biol. *183*, 795–803. https://doi.org/10.1083/jcb.200809125.

48. Igarashi, R., Yamashita, S.I., Yamashita, T., Inoue, K., Fukuda, T., Fukuchi, T., and Kanki, T. (2020). Gemcitabine induces Parkin-independent mitophagy through mitochondrial-resident E3 ligase MUL1-mediated stabilization of PINK1. Sci. Rep. *10*, 1465. https://doi.org/10.1038/s41598-020-58315-w.

49. Oka, T., Sayano, T., Tamai, S., Yokota, S., Kato, H., Fujii, G., and Mihara, K. (2008). Identification of a novel protein MICS1 that is involved in maintenance of mitochondrial morphology and apoptotic release of cytochrome c. Mol. Biol. Cell *19*, 2597–2608. https://doi.org/10.1091/mbc.E07-12-1205.

## STAR★METHODS

### KEY RESOURCES TABLE

| REAGENT or RESOURCE | SOURCE | IDENTIFIER |
|---|---|---|
| Antibodies | | |
| PINK1 | LSBio | Cat#LS-C96472; RRID:AB_10559463 |
| PINK1 | Cell Signaling Technology | Cat#6946; RRID:AB_11179069 |
| TIM23 | BD Biosciences | Cat#611223; RRID:AB_398755 |
| TIM23 | Abgent | Cat#AP14103b;RRID:AB_10892283 |
| TIM22 | Sigma-Aldrich | Cat#T8954; RRID:AB_1858017 |
| TIM17A | Proteintech | Cat#11189-1-AP; RRID:AB_2271661 |
| TIM17A | Ishihara and Mihara[46] | N/A |
| TIM17B | Proteintech | Cat#11062-1-AP; RRID:AB_2201995 |
| TIM50 | Proteintech | Cat#22229-1-AP; RRID:AB_2879039 |
| TIM44 | Proteintech | Cat#13859-1-AP; RRID:AB_2204679 |
| TOM40 | Proteintech | Cat#18409-1-AP; RRID:AB_2303725 |
| OMA1 | Proteintech | Cat#17116-1-AP; RRID:AB_2299053 |
| AFG3L2 | GeneTex | Cat#GTX102036; RRID:AB_11171320 |
| HTRA2 | Proteintech | Cat#15775-1-AP; RRID:AB_2122835 |
| PARL | Proteintech | Cat#26679-1-AP; RRID:AB_2880599 |
| YME1L | Proteintech | Cat#11510-1-AP; RRID:AB_2217459 |
| MIC19 | Sigma-Aldrich | Cat#HPA042935; RRID:AB_10794538 |
| TOM7 | ABclonal | Cat#A17711; RRID:AB_2772682 |
| LETM1 | Sigma-Aldrich | Cat#HPA011029; RRID:AB_1852804 |
| ATP5A1 | Thermo Fisher | Cat#43-9800; RRID:AB_2533548 |
| HSPA9 | Thermo Fisher | Cat#MA3-028; RRID:AB_325474 |
| Actin | Wako Pure Chemicals | Cat#013-24553 |
| Tubulin | Wako Pure Chemicals | Cat#014-25041; RRID:AB_2650453 |
| HA tag | Wako Pure Chemicals | Cat#014-21881 |
| HA tag | Roche | Cat#11867423001; RRID:AB_390918 |
| DYKDDDDK tag (FLAG tag) | Cell Signaling Technology | Cat#14793; RRID:AB_2572291 |
| Parkin | Santa Cruz Biotechnology | Cat#sc-32282; RRID:AB_628104 |
| Chemicals, Peptides, and Recombinant Proteins | | |
| CCCP | Sigma-Aldrich | Cat#C2759 |
| MG132 | Peptide Institutes | Cat#3175-v |
| Bortezomib | Selleck Chemicals | Cat#S1013 |
| TMRM | Sigma-Aldrich | Cat#115532508 |
| MitoBright TL Deep Red | Dojindo | Cat#MT12 |
| Lipofectamine 2000 | Thermo Fisher | Cat#11668019 |
| FuGENE HD | Promega | Cat#E2312 |
| PINK1: AFTSSVPLLPGALVDYPDVLPS[heavy]R | This study | N/A |
| PINK1: APGAPAFPLAI[heavy]K | This study | N/A |
| PINK1: LEEYLIGQSIG[heavy]K | This study | N/A |
| TIM23: YLVQDTDEFILPTGAN[heavy]K | This study | N/A |
| TIM23: ETQNMAWSKP[heavy]R | This study | N/A |
| TIM23: GAEDDLNTVAAGTMTGMLY[heavy]K | This study | N/A |

(*Continued on next page*)

*Continued*

| REAGENT or RESOURCE | SOURCE | IDENTIFIER |
|---|---|---|
| Deposited data | | |
| MS analysis of immunoprecipitated proteins from HeLa cells expressing PINK1-3FLAG | This study | Table S1; ProteomeXchange: JPST002109 |
| Absolute quantification peptide-based quantitative MS analysis of PINK1-3HA and TIM23 | This study | Table S2; ProteomeXchange: JPST002110 |
| Experimental Models: Cell Lines | | |
| GFP-Parkin HeLa cell line | Matsuda et al.[23] | N/A |
| YFP-Parkin HeLa cell line | Narendra et al.[47] | N/A |
| PINK1-3FLAG HeLa cell line | Koyano et al.[11] | N/A |
| PINK1-3HA HeLa cell line | This study | N/A |
| TOM7-KO HeLa cell line | Sekine et al.[24] | N/A |
| PINK1-KO HeLa cell line | Igarashi et al.[48] | N/A |
| Oligonucleotides | | |
| siRNA sequences | This study | Table S3 |
| Recombinant DNA | | |
| pEF1-TIM23-3HA | This study | N/A |
| pEF1-PINK1-3HA | Akabane et al.[30] | N/A |
| pEF1-PINK1(kinase dead)-3HA | This study | N/A |
| pCMVTNT-PINK1-3HA | This study | N/A |
| pCMVTNT-PINK1(A78V)-3HA | This study | N/A |
| pCMVTNT-PINK1(R98W)-3HA | This study | N/A |
| pCMVTNT-PINK1(L347P)-3HA | This study | N/A |
| pCMV(d1)TNT-PINK1-3HA | Okatsu et al.[10] | N/A |
| pCMV(d1)TNT-PINK1(A78V)-3HA | This study | N/A |
| pCMV(d1)TNT-PINK1(R98W)-3HA | This study | N/A |
| pCMV(d1)TNT-PINK1(L347P)-3HA | This study | N/A |
| pEGFP-N1-PINK1-3HA-TEV | This study | N/A |
| p3xFLAG-CMV14-MIC19-3HA-TEV | This study | N/A |

## RESOURCE AVAILABILITY

### Lead contact

Further information and requests for resources and reagents should be directed to and will be fulfilled by the lead contact, Toshihiko Oka (toka@rikkyo.ac.jp).

### Materials availability

All unique reagents generated in this study are available from the lead contact with a completed materials transfer agreement.

### Data and code availability

The proteomics data have been deposited at the ProteomeXchange Consortium via the jPOST partner repository and are publicly available as of the date of publication. Accession numbers are listed in the key resources table. This paper does not report original code. Any additional information required to reanalyze the data reported in this paper is available from the lead contact upon request.

## EXPERIMENTAL MODEL AND SUBJECT DETAILS

### Cell lines

HeLa cell lines used in this study are summarized in this paper's key resources table. All cell lines were maintained at 37°C in Dulbecco's modified Eagle's medium supplemented with 10% fetal bovine serum (FBS) and 4.5 mg/mL glucose. For inhibition of proteasome activities, cells were treated for 4 h with either 50 μM MG132 (Peptide Institutes) or 0.5 μM bortezomib (Selleck Chemicals).

## METHOD DETAILS

### Vital staining of mitochondria

For mitochondrial staining, cells were stained with either 50 nM TMRM (tetramethylrhodamine methyl ester; Sigma-Aldrich) or 1 μM MitoBright TL Deep Red (Dojindo Inc) in the DMEM medium. Live fluorescent images of mitochondrial morphology were obtained using a confocal laser-scanning microscope LSM800 (Carl Zeiss Inc.).

### Analysis of Parkin intracellular localization

For mitochondrial depolarization, cells were treated with 7 or 10 μM CCCP (carbonyl cyanide m-chlorophenylhydrazone; Sigma-Aldrich) and then subjected to immunoblot and microscopic analysis. Intracellular localization of GFP-Parkin was scored under a fluorescence microscope without cell fixation. Data represent the mean ± SEM of three independent experiments; >100 individual cells were counted. Statistical analyses were performed by either one-tailed Student's *t* test or one-way ANOVA with Tukey's multiple comparisons test using GraphPad Prism software.

### DNA and siRNA transfection

The plasmids and siRNA duplexes used in this study are summarized in key resources table. DNA transfection was performed using FuGENE HD (Promega) according to the manufacturer's instructions. After incubation for 48 h, the cells were harvested and used for immunoblot analysis. All siRNA duplexes were transfected into cells using Lipofectamine 2000 (Thermo Fisher) according to the manufacturer's instructions. Cells were transfected twice with the same siRNA at a 48-h interval, incubated further for 48 h, and then subjected to immunoblot analysis and GFP-Parkin recruitment analysis.

### RNA preparation and quantitative PCR

Cells were transfected with the indicated siRNAs, and total RNAs were extracted from the cells with TRIzol reagent (Thermo Fisher), according to the manufacturer's instructions. cDNAs were synthesized from the total RNAs using a ReverTraAce qPCR RT Kit (TOYOBO Life Science). Quantitative PCR was performed as described previously.[48] Data represent the mean ± SEM of three independent experiments. Statistical analyses were performed by one-way ANOVA with Dunnett's multiple comparisons test using BellCurve for Excel version 4.03 (Social Survey Research Information Co., Ltd).

### Immunoblot

Immunoblotting was performed as described previously.[49] For detection of PINK1 phosphorylation, proteins were electrophoresed with acrylamide gels containing 25 μM Phos-tag acrylamide (Wako Pure Chemicals) and 50 μM $MnCl_2$. Before transferring to polyvinylidene difluoride (PVDF) membranes (Merck Millipore), the gels were incubated for 10 min with buffer (20% methanol, 25 mM Tris, 192 mM glycine, and 0.01% SDS) containing 1 mM EDTA, and then washed for 10 min with the same buffer without EDTA. After immunoblotting, the PVDF membranes were incubated with the indicated antibodies, and proteins were detected within a linear detection range using the Novex AP Chemiluminescent substrate (Thermo Fisher) by either ImageQuant 800 (Cytiva) or FUSION Solo 6S EDGE (Vilber Bio Imaging). Antibodies used in this study are summarized in key resources table.

### Clear native PAGE

Clear-native PAGE was performed as described previously.[30] For the native antibody-based mobility shift (NAMOS) assay, the digitonin-solubilized mitochondrial proteins were incubated at 4°C with the indicated antibody, and then subjected to electrophoresis on 4%–16% gradient gels (Thermo Fisher) in the running buffer (50 mM tricine [pH 7.0] and 7.5 mM imidazole) containing 0.05% sodium cholate (Dojindo Laboratories) and 0.01% n-heptyl-β-D-thioglucoside (Dojindo Laboratories). After electrophoresis, proteins in the gels were denatured at 60°C for 20 min with buffer (20 mM Tris-HCl [pH 6.8], 1% SDS, and 0.1 M β-mercaptoethanol), transferred to PVDF membranes, and then subjected to immunoblot analysis.

### Immunoprecipitation

Cells were harvested, washed with phosphate-buffered saline and solubilized at 4°C for 30 min in buffer A (20 mM Tris-HCl [pH 8.0], 100 mM NaCl, and 10% glycerol) containing 1% digitonin. After removal of cell debris by centrifugation, the solubilized proteins were subjected to immunoprecipitation using anti-HA beads (Wako Pure Chemicals) at 4°C for 120 min. The beads were washed twice with buffer A containing 0.25% digitonin, and then washed once with buffer A. The precipitates were subjected to immunoblot analysis. Intensity of bands was quantified using the image analysis software ImageQuant TL version 8.2 (Cytiva). Data represent the mean ± SEM of 3 independent experiments. Statistical significance was determined by one-way ANOVA with Dunnett's multiple comparisons test using GraphPad Prism software.

For ATP depletion, mitochondrial fractions were incubated at 10°C for 20 min with 25 units/ml apyrase, and then solubilized in buffer A containing 1% digitonin. After immunoprecipitating using anti-HA beads, the precipitates were analyzed by SDS-PAGE and immunoblot. For digestion by TEV protease, mitochondrial fractions were prepared from cells expressing both PINK1-3HA-TEV-GFP and MIC19-3HA-TEV-3FLAG, and incubated at 4°C for 60 min with TEV protease (333 units/ml) in buffer B

(50 mM Tris-HCl [pH 8.0], 0.5 mM EDTA, 0.3 M Trehalose). After washing, mitochondrial fractions were solubilized, immunoprecipitated using anti-HA beads, and subjected to immunoblot analysis.

### LC-MS/MS analysis

Control parental HeLa cells and HeLa cells stably expressing PINK1-3FLAG were treated with or without 10 μM CCCP for 3 h, incubated with 0.1% paraformaldehyde for 10 min at room temperature, and then quenched with 100 mM glycine-NaOH (pH7.5) for 4 min. After washing twice with 20 mM HEPES-NaOH (pH7.4) and 137 mM NaCl, the cells were solubilized on ice for 10 min in RIPA buffer (20 mM HEPES-NaOH [pH 7.5], 150 mM NaCl, 1mM $MgCl_2$, 1 mM EGTA, 0.05% SDS, 0.25% sodium deoxycholate, 1% NP-40) supplemented with a protease inhibitor cocktail and 50 unit/ml Benzonase (Merck Millipore), and then subjected to centrifugation (20,000 × g) at 4°C for 15 min. The resultant supernatants were incubated at 4°C for 1 h with anti-FLAG M2 Magnetic Beads (Sigma-Aldrich). The beads were washed 4 times with RIPA buffer and then twice with 50 mM ammonium bicarbonate. Proteins on the beads were digested by adding 200 ng trypsin/Lys-C mix (Promega) at 37°C overnight. The digests were reduced, alkylated, acidified, and desalted with GL-Tip SDB (GL Sciences). The eluates were evaporated and dissolved in 0.1% trifluoroacetic acid and 3% acetonitrile. LC-MS/MS analysis of the resultant peptides was performed on an EASY-nLC 1200 UHPLC connected to a Q Exactive Plus mass spectrometer through a nanoelectrospray ion source (Thermo Fisher). The peptides were separated on a 75-μm inner diameter x 150 mm C18 reversed-phase column (Nikkyo Technos) with a linear 4%–32% acetonitrile gradient for 0–150 min followed by an increase to 80% acetonitrile for 15 min and finally held at 80% acetonitrile for 15 min. The mass spectrometer was operated in data-dependent acquisition mode with the top 10 MS/MS method. MS1 spectra were measured at a resolution of 70,000, an automatic gain control target of 1e6, and a mass range from 350 to 1500 m/z. HCD MS/MS spectra were triggered at a resolution of 17,500, an automatic gain control target of 5e4, an isolation window of 2.0 m/z, a maximum injection time of 60 ms, and a normalized collision energy of 27. Dynamic exclusion was set to 10 s. Raw data were directly analyzed against the SwissProt database restricted to Homo sapiens using Proteome Discoverer 2.4 (Thermo Fisher) with the Sequest HT search engine. The search parameters were as follows: (a) trypsin as an enzyme with up to 2 missed cleavages; (b) precursor mass tolerance of 10 ppm; (c) fragment mass tolerance of 0.02 Da; (d) carbamidomethylation of cysteine as a fixed modification; and (e) acetylation of protein N-terminus and oxidation of methionine as variable modifications. Peptides and proteins were filtered at a false discovery rate (FDR) of 1% using the Percolator node and Protein FDR Validator node, respectively. Label-free quantification was performed based on intensities of precursor ions using the Precursor Ions Quantifier node. Normalization was performed such that the total sum of abundance values for each sample over all peptides was the same.

To quantify TIM23 and PINK1-3HA in the immunoprecipitates, control or PINK1-3HA-expressing HeLa cells were treated with CCCP and subjected to immunoprecipitation with anti-HA antibody bound to magnetic beads. After spiking with 200 fmol stable isotope-labeled AQUA peptides (Cosmo Bio Co Ltd) as standards, proteins on the beads were digested with 400 ng trypsin/LysC mixture at 37°C overnight. The digests were reduced, alkylated, acidified, desalted, evaporated, and dissolved in 0.1% trifluoroacetic acid and 3% acetonitrile. The absolute amounts of tryptic peptides derived from TIM23 and PINK1-3HA were measured by PRM. Targeted MS/MS scans were acquired by a time-scheduled inclusion list at a resolution of 70,000, an AGC target of 2e5, an isolation window of 2.0 m/z, a maximum injection time of 300 ms, and a normalized collision energy of 27. Time alignment and quantification of the transitions of three biological replicates were performed using Skyline software.

## QUANTIFICATIONS AND STATISTICAL ANALYSIS

Statistical analyses were performed using three biological replicates with either GraphPad Prism software or BellCurve for Excel. The data represent the mean ± SEM. Statistical significance was analyzed by one-way ANOVA with either Tukey's multiple comparisons test or Dunnett's multiple comparisons test. For comparison between two groups, data were analyzed with one-tailed Student's *t* test. p values (<0.05) were considered significant.